

Facet-insensitive graphene growth on copper

Xi Mi,^{1,2} Vincent Meunier,^{1,2} Nikhil Koratkar,^{1,3} and Yunfeng Shi^{1,*}

¹*Department of Materials Science and Engineering, Rensselaer Polytechnic Institute, Troy, NY 12180, USA*

²*Department of Physics, Applied Physics, and Astronomy, Rensselaer Polytechnic Institute, Troy, NY 12180, USA*

³*Department of Mechanical, Aerospace & Nuclear Engineering, Rensselaer Polytechnic Institute, Troy, NY 12180, USA*

(Received 19 January 2012; published 19 April 2012)

Polycrystalline copper foils are surprisingly effective in chemical vapor deposition of graphene, although only Cu(111) facets possess the correct symmetry and low lattice mismatch. Density functional theory calculations of carbon on three copper facets show that, as the carbon cluster grows, the carbon-copper interaction weakens while the carbon-carbon interaction strengthens. At a significant distance away, and with negligible electron transfer from the substrate, large carbon clusters are blind to the atomic details of the copper substrates.

DOI: [10.1103/PhysRevB.85.155436](https://doi.org/10.1103/PhysRevB.85.155436)

PACS number(s): 81.05.ue, 82.30.Fi, 31.15.E–

Graphene has drawn substantial interest owing to its remarkable physical properties, such as extremely high electron mobility, zero band gap, and linear electronic band structure dispersion.^{1–7} Few-layered graphene was first obtained through mechanical exfoliation.² However, industrial applications call for more scalable methods that can produce continuous graphene films of high quality over large-area substrates. The chemical vapor deposition (CVD) method has recently become the most promising candidate for graphene synthesis. During CVD growth, gaseous hydrocarbon is thermally decomposed and deposited onto polycrystalline Ni^{8–11} or Cu^{12,13} substrates. Two distinct growth mechanisms exist for Cu and Ni: catalytic, self-limiting graphene growth (monolayer) on polycrystalline Cu; and dissolution-precipitation growth of graphene (few-layer) on Ni.¹⁴ Based on this knowledge, recent experiments used Cu-Ni alloys as substrates for graphene growth to achieve precise control of the number of graphene layers.^{15,16} Several experimental studies have also demonstrated graphene epitaxial growth on single-crystalline transition metals.^{17–27} Based on the idea of epitaxial growth, the graphene lattice must match the lattice of metal substrates. For that reason, metal surfaces that are hexagonal close-packed, such as Cu(111),^{17,18} Ni(111),^{19,20} Ru(0001),^{20–23} Ir(111),^{24,25} and Pt(111),^{20,26,27} have been investigated because they are likely to induce the assembly of sp^2 carbon. Cu(111) is an ideal candidate for this process, since its hexagonal surface lattice has only a slight mismatch ($\sim 3\text{--}4\%$) with the graphene lattice. Therefore, it is puzzling that the aforementioned polycrystalline Cu (i.e., having many surfaces with different crystalline orientations participating in the graphene growth) is known to serve as an effective substrate for uniform graphene growth. A recent experimental study showed graphene overgrown on distinct copper facets and surface steps, suggesting that the continuity of graphene growth is not affected by the copper surfaces.²⁸ Moreover, graphene was shown to grow on a Cu(100) single crystal with a variety of orientations with respect to the copper lattice.²⁹ Nonetheless, the graphene growth is not strictly equivalent among different copper facets. There is experimental evidence suggesting that graphene growth on Cu(111) surfaces is faster and has less defects than other facets, which is likely due to kinetic reasons.^{30,31}

Several simulation works have focused on modeling graphene growth on transition metals. Chen *et al.* found that

carbon dimer nucleation is favored on step edges of Ru(0001) and Ir(111), while on Cu(111), dimers can nucleate on flat surfaces in addition to step edges.³² For carbon clusters larger than dimers, linear structures are more energetically favorable than compact structures on Cu(111).³³ It was also found that C₂₁, a fraction of C₆₀, may be the precursor to graphene on Cu(111).³⁴ For full graphene, the binding to the metal substrate can be weak^{35,36} or strong,³⁶ depending on the metal. Xu *et al.* determined the most favorable configurations for epitaxially aligned single graphene layers on Cu(111) and Ni(111), respectively.³⁷ However, a systematic investigation of the complete growth process on various metal facets (beyond hexagonal close-packed surfaces) is still lacking, which hinders our understanding of the facet-insensitive behavior of graphene growth.

In this work, we carried out first-principles calculations on graphene growth from single carbon atoms and carbon clusters to monolayer graphene film on Cu(001), Cu(110), and Cu(111) surfaces. The adsorption energy, the carbon cluster formation energy, the charge transfer from copper to carbon, and the average height of the carbon clusters are used to characterize the growth of graphene on these three copper surfaces. We found that the graphene growth on all three copper surfaces behaves very similarly beyond the growth stage of carbon chains, thus exhibiting facet-insensitive growth mode.

Our research approach is justified as follows. Although only Cu(001), Cu(110), and Cu(111) surfaces are investigated here, any facet can be in principle decomposed into a superposition of these three low-index facets.³¹ Our choice of modeling copper surfaces without considering surface steps is based on a computational report that showed no preference of graphene nucleation on Cu step edges as compared to flat Cu surfaces.³² Recent experiments also indicated that there is no preferential graphene nucleation on kinks, vacancies, or copper grain boundaries above 900 °C of growth temperature.³¹ Furthermore, our model directly considers carbon atoms on copper surfaces without describing the dehydration reaction of hydrocarbon molecules (methane or ethylene). It has been suggested that single carbon atom is thermodynamically unstable on copper surfaces and that CH_x may be the appropriate active species for graphene growth.³⁸ The simplification here of considering only carbon atoms is appropriate at least for growth conditions with high-pressure hydrocarbon gas and very low-pressure hydrogen

gas, under which carbon atoms/clusters are thermodynamically stable on copper surfaces. In another recent work, a bridging metal structure was proposed as an alternative carbon cluster nucleation scheme to trivial carbon incorporation.³⁹ However, such dramatic metal atom involvement is only an intermediate metastable state during carbon cluster coalescence. Therefore, in thermodynamic equilibrium, carbon clusters without such bridging metal structure should dominate.

We used density functional theory (DFT) calculations as implemented in the *Quantum Espresso* package⁴⁰ within the local density approximation (LDA) and the Perdew-Zunger exchange-correlation functional to investigate the configurations of carbon clusters on copper substrates. Structural relaxations with proper choice of initial configurations were used to determine the equilibrium structures. Kinetic energy cutoffs were chosen as 40 Ry and 300 Ry for plane-wave basis sets and charge density grid, respectively. The charge density distributions are computed using Bader's method.⁴¹ A $5 \times 5 \times 1$ Monkhorst-Pack k -point mesh was used. Gaussian smearing was applied so as to achieve fast convergence. Using such conditions, we computed the lattice constant of bulk Cu to be 3.55 Å, which agrees reasonably well with the experimental value of 3.61 Å.⁴²

Top views of the simulation supercells for Cu(001), Cu(110), and Cu(111) are shown in Fig. 1. Three layers of Cu(001) and Cu(110) slabs and four layers of Cu(111) slabs are used. Vacuum layers over 20 Å are used in the direction normal to the slabs to represent isolated slab-boundary conditions. High-symmetry surface adsorption sites are labeled in Fig. 1 as follows: H (hollow) sites, B (bridge) sites, and T (top) sites. However, due to different surface symmetries, a few additional notations are introduced as follows. For Cu(111), the H sites include H_{fcc} , which sits on top of a third-layer Cu atom, and H_{hcp} , which sits on top of a second-layer Cu atom. For Cu(110), the B sites are subdivided into B_{long} (bridging sites in the middle of a long Cu-Cu pair) and B_{short} (bridging sites in the middle of a short Cu-Cu pair). These high-symmetry adsorption sites are used for the initial guesses for structural relaxation to obtain stable configurations of C clusters.

Single C adsorptions on fixed Cu substrates were investigated first. Adsorption energies E_a , atomic heights h (with respect to the top layer of copper atoms), and the electrons transferred (Q) to C atom were calculated for all symmetry sites, as shown in Table I. E_a is defined as the per-atom total energy difference before and after adsorption:

$$E_a = 1/N(E_{\text{C_Cluster}} + E_{\text{Cu_Substrate}} - E_{\text{Cluster_on_Substrate}}) \quad (1)$$

where N is the number of carbon atoms in the cluster, $E_{\text{Cluster_on_Substrate}}$ is the total energy of the system of the carbon cluster adsorbed on Cu substrate, $E_{\text{C_Cluster}}$ is the energy of the isolated carbon cluster, and $E_{\text{Cu_Substrate}}$ is the energy of isolated Cu substrate. Note that a positive adsorption energy indicates an exothermic and favorable adsorption process.

Table I indicates that single C adsorptions at H sites on Cu(001), B_{long} sites on Cu(110), and H sites (both H_{fcc} and H_{hcp}) on Cu(111) have the highest adsorption energy, largest

amount of charge transfer, and shortest vertical separation from the metal substrate. Our results agree reasonably well with other works in terms of E_a at H sites on Cu(111).³² E_a , h , and Q for the T sites on Cu(001), Cu(110), and Cu(111) are consistent, as the C adatom only interacts with one copper atom in each case. Results for the B site on Cu(001), B_{short} site on Cu(110), and B site on Cu(111) are all mutually consistent because of the similar chemical environment for the carbon adatom in each case. We also carried out DFT calculations, in which the Cu substrates are allowed to relax: a single carbon on the H site of Cu(001), B_{long} site of Cu(110), and H_{fcc} site of Cu(111). For each of these systems, only the bottom copper layer is constrained, and all the other layers are free to relax. In addition, we simulated single-carbon adsorptions on six-layer copper substrates for comparison in order to verify the choice of thin copper slabs. For each of these systems, the bottom three layers are fixed, and the top three layers are unconstrained. The results are also listed in Table I and agree reasonably well with samples with fixed substrates in terms of E_a , h , and Q . Therefore, rigid Cu substrates with 3–4 layers are used throughout the rest of the paper.

To investigate carbon clusters with different sizes on Cu substrates, we systematically set up multiple systems with various cluster configurations on Cu(001), Cu(110), and Cu(111) surfaces, shown and numbered in Fig. 2. Due to the vast amount of possible cluster configurations on copper surfaces, we used the following recursive scheme to identify stable cluster configurations. To construct a C cluster consisting of $N + 1$ atoms ($N = 1, 2, \dots$), a known stable configuration of a carbon cluster with N atoms (obtained from the last iteration) is selected. Then, the $(N + 1)$ th carbon atom is assigned to one of the nearby high-symmetry sites. Next, a structural relaxation is performed to rearrange the cluster into a stable configuration. Finally, two to three most energetically stable clusters with $N + 1$ carbon atoms are selected to serve as the initial configurations for the next iteration. Other energetically unfavorable configurations are discarded. Note that an exhaustive search is beyond the computational capacity available today. Nonetheless, the cluster configurations considered here are representative as a result of screening the cluster configurations based on chemistry and symmetry. The samples we generated this way represent the most probable cluster configurations under experimental conditions. Starting from carbon monomers ($N = 1$), we produced carbon dimers ($N = 2$), trimers ($N = 3$), and tetramers ($N = 4$) by this recursive method. In addition, once small clusters are built, C chains are obtained by elongating linear C tetramers to attach their periodic images. Linear carbon chains are usually formed upon relaxation, which is consistent with results from the literature.³³ Finally, monolayer graphene on different Cu substrates are constructed. For Cu(111), we assumed perfect alignment of graphene layers on Cu(111) (sample 62 and 63), similar to previous works.³⁷ For Cu(001) and Cu(110), much larger supercells were selected to match the periodicities of both the copper surfaces and graphene (sample 20 and 40 in Fig. 2). In all cases, the lattice mismatch between graphene and the copper substrate is less than 3%.

We used the cluster formation energy per atom (E_{form}) to describe the thermodynamic driving force for aggregation of isolated carbon atoms adsorbed on copper, by generalizing the

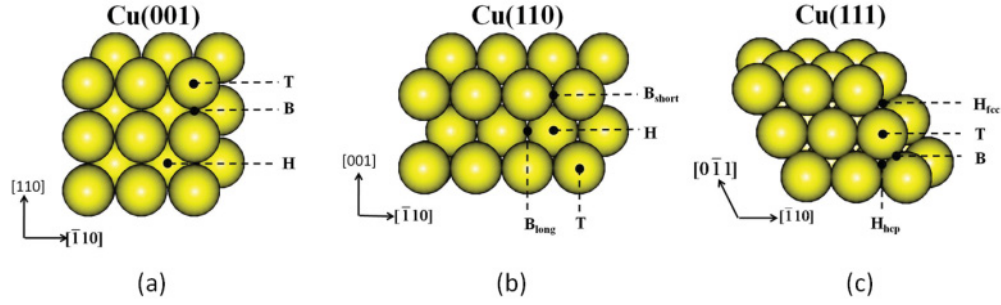


FIG. 1. (Color online) Surface unit cells for (a) Cu(001), (b) Cu(110), and (c) Cu(111) slabs. Crystal directions and high-symmetric sites are noted.

dimer formation energy.³² The cluster formation energy E_{form} is defined as the amount of formation energy per carbon atom of a carbon cluster on copper, from isolated carbon atoms absorbed on preferred adsorption sites:

$$E_{\text{form}} = 1/N(E_{\text{Cu_Substrate}} + N \cdot E_C - N \cdot E_a^C - E_{\text{Cluster_on_Substrate}}) \quad (2)$$

where E_C is the energy of a single isolated carbon atom. The binding energies of C monomers E_a^C are taken as the highest adsorption energies for single carbon on each respective Cu substrate. It is equal to $E_a(\text{H})$ on Cu(001), $E_a(\text{B}_{\text{long}})$ on Cu(110), or $E_a(\text{H}_{\text{fcc}})$ on Cu(111), respectively.

In Fig. 3(a), (b), (c), and (d), E_a , E_{form} , h , and Q as a function of CN_{C-C} (the average number of neighboring carbon atoms) are plotted for all C cluster structures, respectively. CN_{C-C} is used here to characterize the extent of growth of carbon clusters. Each data point corresponds to one simulated system in Fig. 2. Note that the dashed lines in Fig. 3 connect data of the energetically favorable configurations at different growth stages (cluster sizes) on different copper surfaces. The process outlined by those favorable cluster configurations shows that, as growth proceeds: the adsorption energy E_a decreases, the cluster formation energy E_{form} increases, the cluster height h increases, and the charge transfer per atom Q decreases. These trends can be clearly seen for all three copper surfaces investigated here. Therefore, regardless of the type of the Cu facets, the C-Cu interactions weaken as the carbon cluster grows.

Careful examination of Fig. 3 allows us to divide the growth process into a facet-sensitive stage and a facet-insensitive stage. On one hand, for $CN_{C-C} = 0$ (C monomer) and

$CN_{C-C} = 1$ (C dimer), the adsorption energy is substantial (E_a around a few electron volts per atom), and charge transfer is significant (Q is more than 0.5 e/atom). Moreover, E_a can differ by ~ 1 eV/atom for different Cu facets, which indicates that C-Cu interactions are not only strong but also facet sensitive. On the other hand, for all Cu facets at $CN_{C-C} = 2$ (C chain), E_a converges to ~ 0.2 eV/atom and Q to ~ 0.1 e/atom. For all Cu facets at $CN_{C-C} = 3$ (graphene layer), E_a converges to less than 0.1 eV/atom, and there is negligible charge transfer $Q \sim 0$. Therefore, away from the copper substrate and absent of charge transfer, carbon chains and graphene flakes interact weakly with the copper substrate, and thus are indifferent to various crystallographic planes. Due to such a weak interaction, the graphene flakes are likely to rotate and realign at high temperature upon coalescence.⁴³ For the same reason, graphene is unlikely to adopt any particular relative orientation with respect to copper substrate or be strained even with lattice mismatch. It should be noted that the absolute cluster formation energies for $CN_{C-C} = 2$ and 3 are indeed facet-dependent, which is due to the facet-sensitive adsorption energy for isolated carbons [as in Eq. (2)]. However, the difference in formation energy, such as $E_{\text{form}}(CN_{C-C} = 3) - E_{\text{form}}(CN_{C-C} = 2)$, which characterizes the thermodynamic driving force from carbon chain to graphene, is still facet-insensitive.

The evolution of C-Cu interactions with increasing CN_{C-C} is also illustrated in the charge difference density plots (Fig. 4) for a single C atom (sample 41), C dimer (sample 46), C chain (sample 61), and a single graphene layer (sample 63) on Cu(111). The charge density changes are calculated as $\Delta\rho = (\rho_{\text{Cu_Substrate}} - \rho_{\text{IsolatedCarbons}} - \rho_{\text{IsolatedSubstrate}})$ so as to

TABLE I. Adsorption energies E_a , heights h , and charge transfer Q for single-carbon-atom adsorption on fixed Cu(001), Cu(110), and Cu(111) substrates. The preferred adsorption sites are also calculated for relaxed copper substrates (noted with the superscript 'r'). Samples with thin copper slab (three or four layers of Cu) are at the top, and samples with thick copper slab (six layers of Cu) are at the bottom.

	Cu(001)				Cu(110)					Cu(111)				
	T	B	H	H ^r	T	B _{short}	H	B _{long}	B _{long} ^r	T	B	H _{hcp}	H _{fcc}	H _{fcc} ^r
E_a (eV)	3.18	4.40	6.33	6.54	3.11	4.32	5.50	5.72	5.85	3.21	4.60	5.03	5.07	5.17
				6.53					5.85					5.17
h (Å)	1.75	1.31	0.61	0.36	1.74	1.30	0.58	0.35	0.23	1.75	1.29	1.15	1.15	1.10
				0.31					0.22					1.11
Q (e)	0.39	0.60	0.99	1.00	0.37	0.54	0.77	0.82	0.83	0.39	0.60	0.65	0.68	0.70
				1.02					0.81					0.70

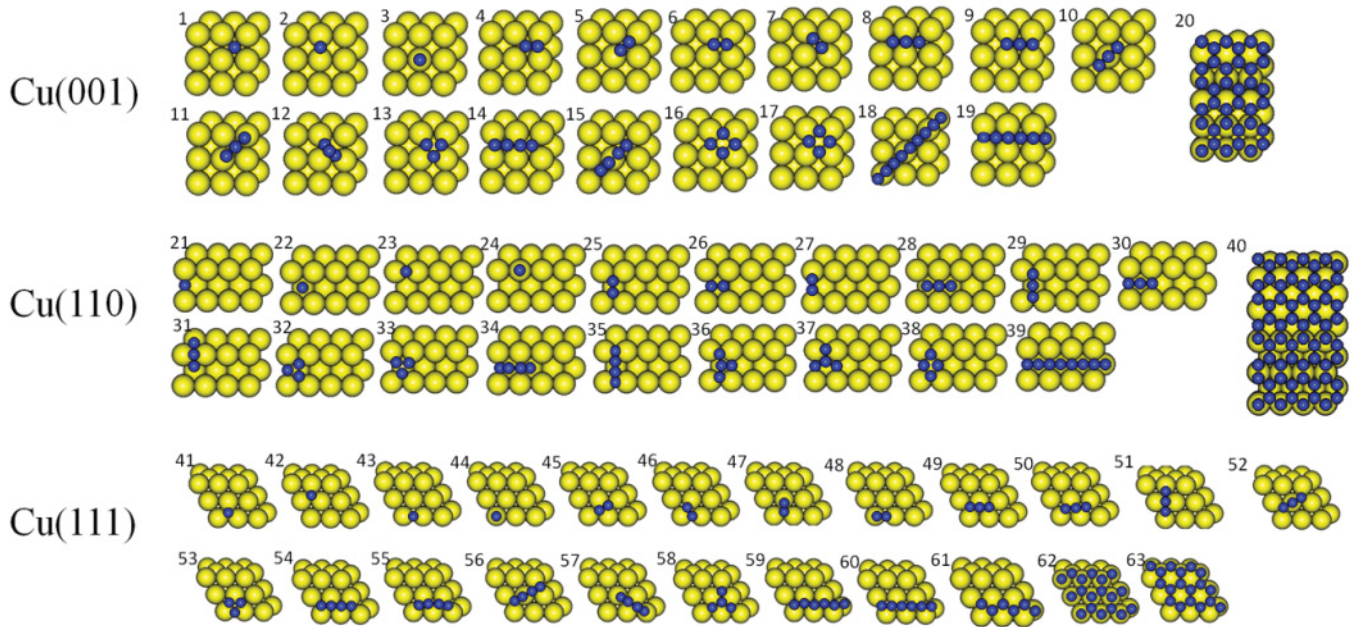


FIG. 2. (Color online) Top views for equilibrium structural configurations of different C clusters on Cu(001), Cu(110), and Cu(111). Copper and carbon atoms are colored in yellow/light gray and blue/dark gray, respectively. Unit cells (sample 20 and sample 40) of graphene on Cu(001) and Cu(110) are chosen as such to ensure very low strain in graphene (less than 3%).

reveal both the Cu-C bonding and C-C bonding. In Fig. 4(a), a single carbon atom is bonded covalently with all of its three neighboring Cu atoms, with electron transfer from copper to

carbon. As carbon clusters grow larger, the charge transfer from copper to carbon progressively vanishes. At the same time, electron transfer occurs from carbon atoms to form strong

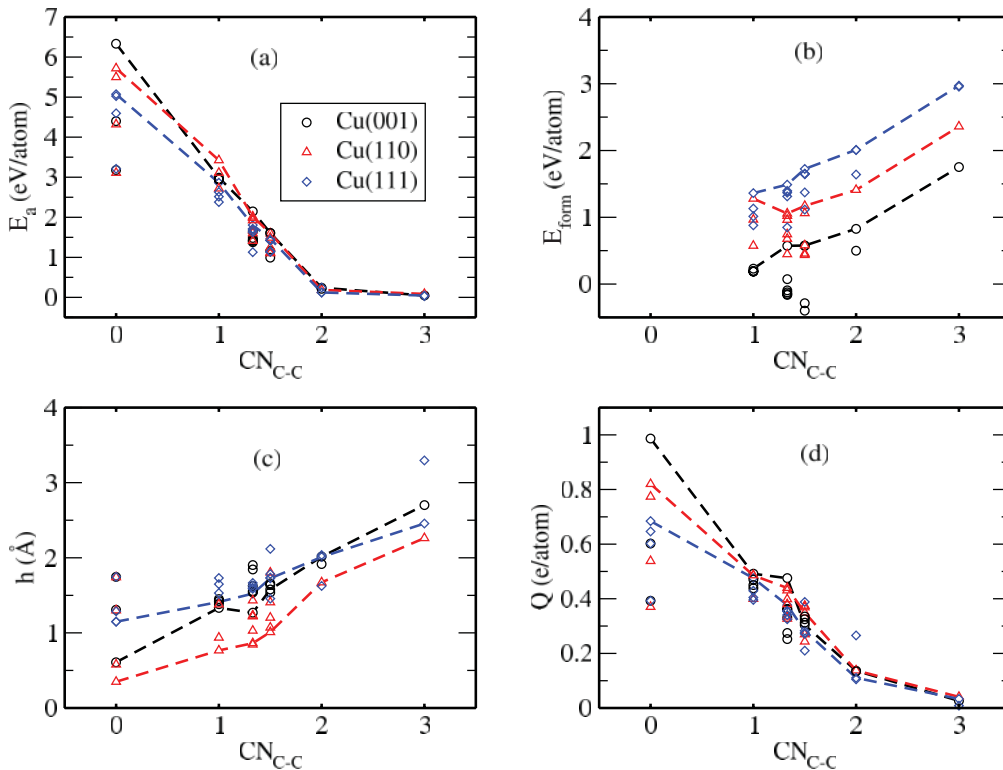


FIG. 3. (Color online) (a) Adsorption energies per atom, (b) formation energies per atom, (c) averaged heights, and (d) average transferred charges vs CN_{C-C} . Results on Cu(001), Cu(110), and Cu(111) are represented by black circles, red triangles, and blue diamonds, respectively. The dashed lines envelop the most energetically stable configurations at different growth stages on various copper surfaces, in order to guide the eye.

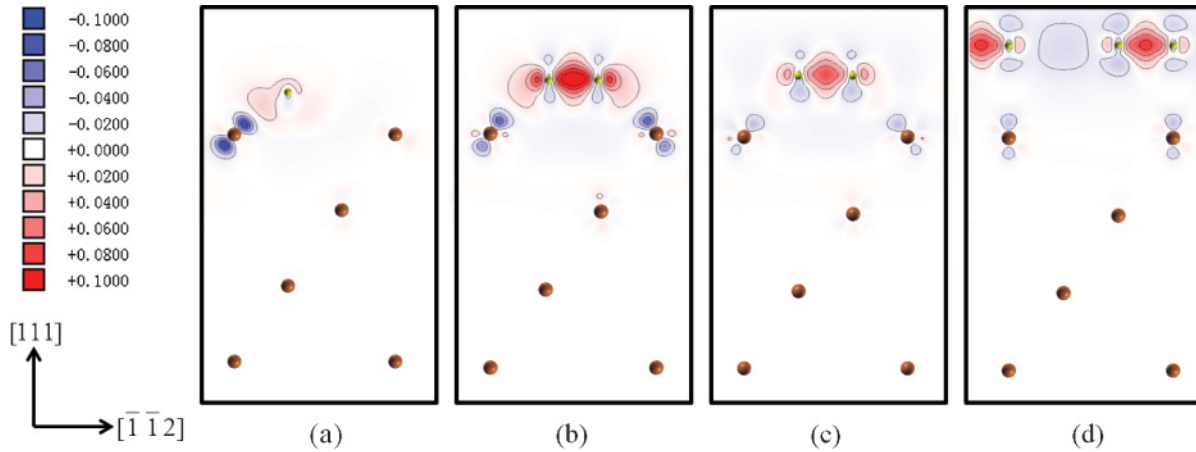


FIG. 4. (Color online) Cross-section views of the charge difference density maps (formula is in the main text) of carbon on Cu(111): (a) single C, (b) C dimer, (c) C chain, and (d) graphene layer. These plots correspond to samples 41, 46, 61, and 63 on Fig. 2, respectively. Cu atoms are colored in brown/medium gray, and carbon atoms are colored in yellow/light gray. Note that not all atoms of the supercell are on the selected cross-section. $-/+$ represent the electron loss/gain. The unit for charge density is electrons per cubic Bohr radius. The overall charge transfer is 0.68, 0.48, 0.11, and 0.03 e per carbon atom for panes (a) to (d).

C-C covalent bonds. In Fig. 4(d), Cu-C interactions become almost negligible. The carbon atoms move away from the substrate, as shown in Fig. 4. It can be concluded that carbon atoms prefer to form bonds with other carbon atoms than with Cu atoms. The preference of C-C bonding over C-Cu bonding leads to bond switching from C-Cu to C-C as the carbon cluster grows.

Based on the results explained here, the general mechanism of surface-insensitive growth of graphene on Cu can be understood as follows. At the initial growth stage, where C monomers and C dimers dominate, C-Cu interactions are surface dependent because carbon atoms form C-Cu bonds as well as C-C bonds. When growth proceeds, C atoms preferably form covalent bonds with other carbon atoms and at the same time break bonds with Cu atoms due to saturation of covalent bonds. Once C chains emerge, C-Cu interactions switch to nonbonding interactions, which are not only weaker but also have a larger equilibrium separation. The growth then becomes surface-insensitive. Thus, C chains are expected to be much more mobile than smaller clusters, which are crucial for the later-stage graphene growth.

In summary, we have obtained minimum energy configurations for various C clusters on Cu(001), Cu(110), and Cu(111)

in a recursive manner. It was found that, regardless of the type of Cu facet substrate, C clusters and Cu substrates interact more weakly (lower adsorption energy, lower charge transfer, and a larger separation) as the carbon cluster grows. At a significant distance away from the substrate without electron transfer, large carbon clusters are blind to the atomic details of the copper substrate. At the same time, the carbon cluster formation energy increases as graphene growth proceeds. It is the bond switching from C-Cu to C-C that leads to the facet-insensitive graphene growth on copper.

ACKNOWLEDGMENTS

We thank the Advanced Energy Consortium (AEC) for funding support. We are also grateful for the stimulating discussions with Qingkai Yu (Texas State University), Shengbai Zhang (Rensselaer Polytechnic Institute), Angel Garcia (Rensselaer Polytechnic Institute), Jie Lian (Rensselaer Polytechnic Institute), Liping Huang (Rensselaer Polytechnic Institute), and Pulickel Ajayan (Rice University). Numerical simulations were carried out on supercomputers in the Computational Center for Nanotechnology Innovations (CCNI) at Rensselaer Polytechnic Institute.

*shiy2@rpi.edu

¹A. K. Geim and K. S. Novoselov, *Nat. Mater.* **6**, 183 (2007).

²K. S. Novoselov, *Science* **306**, 666 (2004).

³A. K. Geim, *Science* **324**, 1530 (2009).

⁴D. S. L. Abergel, V. Apalkov, J. Berashevich, K. Ziegler, and T. Chakraborty, *Adv. Phys.* **59**, 261 (2010).

⁵A. H. Castro Neto, F. Guinea, N. M. R. Peres, K. S. Novoselov, and A. K. Geim, *Rev. Mod. Phys.* **81**, 109 (2009).

⁶K. S. Novoselov, A. K. Geim, S. V. Morozov, D. Jiang, M. I. Katsnelson, I. V. Grigorieva, S. V. Dubonos, and A. A. Firsov, *Nature* **438**, 197 (2005).

⁷Y. Zhang, Y. W. Tan, H. L. Stormer, and P. Kim, *Nature* **438**, 201 (2005).

⁸Q. Yu, J. Lian, S. Siriponglert, H. Li, Y. P. Chen, and S. S. Pei, *Appl. Phys. Lett.* **93**, 113103 (2008).

⁹A. Reina, X. Jia, J. Ho, D. Nezich, H. Son, V. Bulovic, M. S. Dresselhaus, and J. Kong, *Nano Lett.* **9**, 30 (2009).

¹⁰K. S. Kim, Y. Zhao, H. Jang, S. Y. Lee, J. M. Kim, K. S. Kim, J. H. Ahn, P. Kim, J. Y. Choi, and B. H. Hong, *Nature* **457**, 706 (2009).

¹¹S. Chae, F. Gunes, K. Kim, E. Kim, G. Han, S. Kim, H. Shin, S. Yoon, J. Choi, M. Park, C. Yang, D. Pribat, and Y. Lee, *Adv. Mater.* **21**, 2328 (2009).

- ¹²X. Li, W. Cai, J. An, S. Kim, J. Nah, D. Yang, R. Piner, A. Velamakanni, I. Jung, E. Tutuc, S. K. Banerjee, L. Colombo, and R. S. Ruoff, *Science* **324**, 1312 (2009).
- ¹³L. Gao, W. Ren, J. Zhao, L.-P. Ma, Z. Chen, and H. M. Cheng, *Appl. Phys. Lett.* **97**, 183109 (2010).
- ¹⁴X. Li, W. Cai, L. Colombo, and R. S. Ruoff, *Nano Lett.* **9**, 4268 (2009).
- ¹⁵S. Chen, W. Cai, R. D. Piner, J. W. Suk, Y. Wu, Y. Ren, J. Kang, and R. S. Ruoff, *Nano Lett.* **11**, 3519 (2011).
- ¹⁶X. Liu, L. Fu, N. Liu, T. Gao, Y. Zhang, L. Liao, and Z. Liu, *J. Phys. Chem. C* **115**, 11976 (2011).
- ¹⁷L. Gao, J. R. Guest, and N. P. Guisinger, *Nano Lett.* **10**, 3512 (2010).
- ¹⁸K. M. Reddy, A. D. Gledhill, C.-H. Chen, J. M. Drexler, and N. P. Padture, *Appl. Phys. Lett.* **98**, 113117 (2011).
- ¹⁹J. Lahiri, T. S. Miller, A. J. Ross, L. Adamska, I. I. Oleynik, and M. Batzill, *New J. Phys.* **13**, 025001 (2011).
- ²⁰M. Gao, Y. Pan, C. Zhang, H. Hu, R. Yang, H. Lu, J. Cai, S. Du, F. Liu, and H. J. Gao, *Appl. Phys. Lett.* **96**, 053109 (2010).
- ²¹P. W. Sutter, J. I. Flege, and E. A. Sutter, *Nat. Mater.* **7**, 406 (2008).
- ²²H. Zhang, Q. Fu, Y. Cui, D. Tan, and X. Bao, *J. Phys. Chem. C* **113**, 8296 (2009).
- ²³D. Martoccia, P. R. Willmott, T. Brugger, M. Björck, S. Günther, C. M. Schlepütz, A. Cervellino, S. A. Pauli, B. D. Patterson, S. Marchini, J. Wintterlin, W. Moritz, and T. Greber, *Phys. Rev. Lett.* **101**, 126102 (2008).
- ²⁴J. Coraux, A. T. N'Diaye, M. Engler, C. Busse, D. Wall, N. Buckanie, F.-J. Meyer zu Heringdorf, R. van Gastel, B. Poelsema, and T. Michely, *New J. Phys.* **11**, 023006 (2009).
- ²⁵S. Nie, A. L. Walter, N. C. Bartelt, E. Starodub, A. Bostwick, E. Rotenberg, and K. F. McCarty, *ACS Nano* **5**, 2298 (2011).
- ²⁶M. Gao, Y. Pan, L. Huang, H. Hu, L. Z. Zhang, H. M. Guo, S. X. Du, and H. J. Gao, *Appl. Phys. Lett.* **98**, 033101 (2011).
- ²⁷P. Sutter, J. T. Sadowski, and E. Sutter, *Phys. Rev. B* **80**, 245411 (2009).
- ²⁸H. I. Rasool, E. B. Song, M. J. Allen, J. K. Wassei, R. B. Kaner, K. L. Wang, B. H. Weiller, and J. K. Gimzewski, *Nano Lett.* **11**, 251 (2011).
- ²⁹H. I. Rasool, E. B. Song, M. Mecklenburg, C. Regan, K. L. Wang, B. H. Weiller, and J. K. Gimzewski, *J. Am. Chem. Soc.* **133**, 12536 (2011).
- ³⁰M. Ishihara, Y. Koga, J. Kim, K. Tsugawa, and M. Hasegawa, *Mater. Lett.* **65**, 2864 (2011).
- ³¹J. D. Wood, S. W. Schmucker, A. S. Lyons, E. Pop, and J. W. Lyding, *Nano Lett.* **11**, 4547 (2011).
- ³²H. Chen, W. Zhu, and Z. Zhang, *Phys. Rev. Lett.* **104**, 186101 (2010).
- ³³R. G. Van Wesep, H. Chen, W. Zhu, and Z. Zhang, *J. Chem. Phys.* **134**, 171105 (2011).
- ³⁴Q. Yuan, J. Gao, H. Shu, J. Zhao, X. Chen, and F. Ding, *J. Am. Chem. Soc.* **134**, 2970 (2012).
- ³⁵M. Vanin, J. J. Mortensen, A. K. Kelkkanen, J. M. Garcia-Lastra, K. S. Thygesen, and K. W. Jacobsen, *Phys. Rev. B* **81**, 081408 (2010).
- ³⁶C. Gong, G. Lee, B. Shan, E. M. Vogel, R. M. Wallace, and K. Cho, *J. Appl. Phys.* **108**, 123711 (2010).
- ³⁷Z. Xu and M. J. Buehler, *J. Phys.: Condens. Matter* **22**, 485301 (2010).
- ³⁸W. Zhang, P. Wu, Z. Li, and J. Yang, *J. Phys. Chem. C* **115**, 17782 (2011).
- ³⁹P. Wu, W. Zhang, Z. Li, J. Yang, and J. G. Hou, *J. Chem. Phys.* **133**, 071101 (2010).
- ⁴⁰P. Giannozzi, S. Baroni, N. Bonini, M. Calandra, R. Car, C. Cavazzoni, D. Ceresoli, G. L. Chiarotti, M. Cococcioni, I. Dabo, A. Dal Corso, S. de Gironcoli, S. Fabris, G. Fratesi, R. Gebauer, U. Gerstmann, C. Gougoussis, A. Kokalj, M. Lazzeri, L. Martin-Samos, N. Marzari, F. Mauri, R. Mazzarello, S. Paolini, A. Pasquarello, L. Paulatto, C. Sbraccia, S. Scandolo, G. Sclauzero, A. P. Seitsonen, A. Smogunov, P. Umari, and R. M. Wentzcovitch, *J. Phys. Condens. Matter* **21**, 395502 (2009).
- ⁴¹W. Tang, E. Sanville, and G. Henkelman, *J. Phys.: Condensed Matter* **21**, 084204 (2009).
- ⁴²N. J. Simon, E. S. Drexler, and R. P. Reed, *Properties of Copper and Copper Alloys at Cryogenic Temperatures* (International Copper Association, Ltd., New York and National Institute of Standards and Technology, Gaithersburg, 1992).
- ⁴³Q. Yu, L. A. Jauregui, W. Wu, R. Colby, J. Tian, Z. Su, H. Cao, Z. Liu, D. Pandey, D. Wei, T. F. Chung, P. Peng, N. P. Guisinger, E. A. Stach, J. Bao, S.-S. Pei, and Y. P. Chen, *Nat. Mater.* **10**, 443 (2011).